Extension of charge-state-distribution calculations for ion-solid collisions towards low velocities and many-electron ions

E. Lamour,[1,2] P. D. Fainstein,[3] M. Galassi,[4] C. Prigent,[1,2] C. A. Ramirez,[4] R. D. Rivarola,[4] J.-P. Rozet,[1,2] M. Trassinelli,[1,2] and D. Vernhet[1,2,*]

[1]*CNRS, UMR 7588, Institut des NanoSciences de Paris (INSP), 4 Place Jussieu, 75005 Paris, France*

[2]*Sorbonne Universités, UPMC Université Paris 06, INSP, UMR 7588, F-75005 Paris, France*

[3]*Centro Atómico Bariloche, Comisión Nacional de Energía Atómica and Consejo Nacional de Investigaciones Científicas y Técnicas (CONICET), 8400 San Carlos de Bariloche, Río Negro, Argentina*

[4]*Laboratorio de Colisiones Atómicas, Instituto de Física Rosario (CONICET-UNR) and Facultad de Ciencias Exactas, Ingeniería y Agrimensura, Universidad Nacional de Rosario, Avenida Pellegrini 250, 2000 Rosario, Argentina*

(Received 4 June 2015; published 12 October 2015)

Knowledge of the detailed evolution of the whole charge-state distribution of projectile ions colliding with targets is required in several fields of research such as material science and atomic and nuclear physics but also in accelerator physics, and in particular in regard to the several foreseen large-scale facilities. However, there is a lack of data for collisions in the nonperturbative energy domain and that involve many-electron projectiles. Starting from the ETACHA model we developed [Rozet *et al.*, Nucl. Instrum. Methods Phys. Res., Sect. B **107**, 67 (1996)], we present an extension of its validity domain towards lower velocities and larger distortions. Moreover, the system of rate equations is able to take into account ions with up to 60 orbital states of electrons. The computed data from the different new versions of the ETACHA code are compared to some test collision systems. The improvements made are clearly illustrated by 28.9 MeV u^{-1} Pb^{56+} ions, and laser-generated carbon ion beams of 0.045 to 0.5 MeV u^{-1}, passing through carbon or aluminum targets, respectively. Hence, those new developments can efficiently sustain the experimental programs that are currently in progress on the "next-generation" accelerators or laser facilities.

DOI: 10.1103/PhysRevA.92.042703 PACS number(s): 34.10.+x, 34.50.Fa

I. INTRODUCTION

Ab initio calculations of charge-state distributions of fast ions at the exit of solid targets are useful in many circumstances, as in the context of energy loss in matter and for the design, or analysis, of atomic or nuclear physics experiments. Several empirical or semiempirical laws can be used to predict the mean charge state at equilibrium and, to some extent, their widths [1,2]. However, not only is the equilibrium charge state or the mean charge state for a given solid target thickness needed, but also the detailed evolution of the whole charge-state distribution as a function of the solid target thickness or even the evolution of the $n\ell$ substate populations. Some explicit charge-state models may provide those types of output, but are limited to few-electron ions: for instance, two programs have been developed by Scheidenberger *et al.* [3] to fulfil this task: CHARGE is a three-state model, and GLOBAL a 28-state model, but excited-state effects are treated only in an approximate way ("quasiground-state model"). The ETACHA code [4] that we initially developed was devoted to calculating charge-state distributions of fast few-electron ions with at most 28 orbital states of electrons. Taking explicitly into account excited-state effects by solving a set of 84 coupled differential equations, it was based on the calculation of cross sections for monoelectronic atomic collision processes in the independent-electron approximation and at high velocities. Therefore, within this version, perturbative theories were used to account for electron capture and intra- and intershell excitation as well as ionization processes. However, many experiments address the nonperturbative regime where the ion stopping power is at maximum, in particular for studies of material damage [5], including biological material that takes advantage of the so-called "Bragg peak" [6,7]. Moreover, there are, at present, active research programs on the production of superheavy elements as at the SPIRAL2 facility [8] and on plasma physics to characterize warm dense matter using intense lasers or the x-ray free-electron laser (XFEL) [9] that need reliable predictions of the projectile charge-state distribution or even of its $n\ell$ substate populations after passing through solid targets. It follows that many studies refer to the ETACHA code (see, e.g., [10,11]), sometimes using its cross-section calculation routines as an input for Monte Carlo approaches [12], and using it in some cases outside its range of validity. There is obviously a need for an extension of ETACHA towards lower velocities and many-electron ions. Similarly, extending the code towards relativistic energies or dealing with gas targets is desirable; these issues will not be addressed in the present study and will come later on.

Two types of change have been made at present. First, since previously used high-velocity theories such as Born1-type calculations for electron loss or excitation break down, more sophisticated theories are needed and have been included in the present version of the code. The question of the validity of using high-velocity theory to describe the capture process also arises. Second, when dealing with more dressed-ions, the basis of projectile states has to be enlarged. Solving these issues is far from simple. In this paper, we present several improvements that have been made to extend the code to 60 orbital states of electrons (up to the $n = 4$ shell) that are passing through solid foils at relatively low velocity, i.e., the collision domain corresponding to the nonperturbative regime. Section IIA will

*Corresponding author: dominique.vernhet@insp.jussieu.fr

present the changes which have been made to the rate equations and associated configurations. Section IIB will deal with new calculations of cross sections, with a short description of the theories that are now included in ETACHA, and a discussion of mean charge-state effects on cross-section values. Some computing aspects are given in Sec. IIC. Finally, in Sec. III, we compare the different versions of the ETACHA code for some test collision systems, demonstrating the improvements that have been made but also exhibiting the validity domain of each version of the ETACHA code, which depends on the number of states with noncorrelated or correlated configurations that have been included.

II. DESCRIPTION OF THE IMPROVED MODELING

We recall here for self-consistency the main features of the model already given in our previous paper [4]. Calculation of projectile charge-state distributions as a function of penetration depth x in the target is performed by solving a set of differential ("rate") equations of the type

$$\frac{dY_i(x)}{dx} = \sum_j Y_j(x)\sigma_{ji} - \sum_j Y_i(x)\sigma_{ij}, \qquad (1)$$

where $Y_i(x)$ stands for the fraction of ions in a specific i state, and σ_{ij} for collision cross sections or transition rates from state i to state j. In this section, we first discuss the number and characteristics of fractions to be considered to treat heavy ions up to 60 orbital states of electrons. Cross sections for extending the validity regime towards the nonperturbative velocity regime and properly accounting for many-electron ions will be discussed in the following sections.

A. Rate equations and configurations

In a ground-state model, cross sections depend only on the total number of electrons (or holes). Then one has just to solve a set of equations whose number corresponds to the electron number that has to be considered. However, a process such as ionization or electron capture is clearly very different for ground-state ions and excited ones, with typical and simple examples being $1s^2$ compared to $1s2s$ or $2s2p$ states. Accordingly, we consider configurations with electrons in well-defined substates instead of the fraction of ions with a given number of electrons. These configurations are more or less numerous, depending on the maximum principal quantum number considered in the calculation.

The simplest model would consider the $n = 1$ shell only, with the three possible configurations corresponding to 0, 1, or 2 electrons in this shell. Going up to $n = 2$, there are three possibilities for the $2s$ subshell and seven $(0,1,\ldots,6$ electrons) for $2p$, that can be either populated or depleted by electron capture or intra- or intershell excitation and ionization processes, as schematically depicted in Fig. 1. It follows that when considering, for instance, states up to $n = 3$, with a maximum number of 28 electrons on the ion, configurations should be of the type $Y(n_{1s},n_{2s},n_{2p},n_{3s},n_{3p},n_{3d},x)$, corresponding to $3\times3\times7\times3\times7\times11 = 14\,553$ configurations, and even many more, if spin dependence and couplings are taken into account. Nevertheless, as discussed in our previous papers [4,13], coupling effects are shown to play a minor role when only

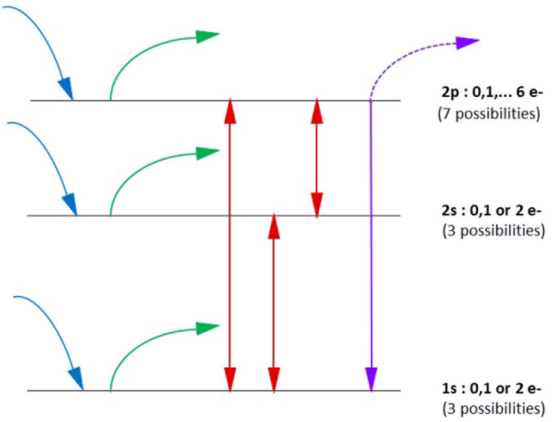

FIG. 1. (Color online) Scheme of the different electronic processes that affect the $n\ell$ state population; from left to right: capture, ionization, inter- and intrashell excitation or radiative decay, and Auger deexcitation.

charge states are considered. Even so, this is far too many configurations if we want to keep the calculation fast enough. Calling such configurations "correlated configurations," an extreme simplification consists in using completely uncorrelated fractions, by calculating independently the fraction of ions with a given number of electrons in a given substate and combining them to obtain an approximation of the previous configurations:

$$Y(n_{1s},n_{2s},n_{2p},n_{3s},n_{3p},n_{3d}) \approx Y(n_{1s})\,Y(n_{2s})\,Y(n_{2p})\,Y(n_{3s})\,Y(n_{3p})\,Y(n_{3d}), \qquad (2)$$

where the target thickness dependence has been omitted for the sake of clarity. This reduces the number of fractions (and coupled equations) to be calculated to $3+3+7+3+7+11 = 34$. Comparison with experiment, however, shows that much better results are obtained by using a slightly more sophisticated scheme. For instance, our previous model [4] uses instead the $3\times3\times7 = 63$ correlated configurations of the type $Y(n_{1s},n_{2s},n_{2p},x)$ for inner shells $n = 1$ and $n = 2$, which were combined with the $3+7+11 = 21$ uncorrelated fractions for $3s$, $3p$, and $3d$ substates. It leads to $63+21 = 84$ fractions that are calculated in this previous version of the ETACHA code, which we now call "ETACHA23."

Among our new modeling developments a version which is still limited to 28 projectile orbital states of electrons uses however a further improvement by considering the $11\times19 = 209$ configurations of the type $Y(n_{12},n_3,x)$, where n_{12} is the total number of electrons in the K and L shells (between 0 and 10) and n_3 the number of M-shell electrons (between 0 and 18). This means that the evolutions with target thickness of $84+209 = 293$ fractions are calculated, in what we call the "ETACHA3" code (see Table I). Note that the 84 fractions of the previous version are kept to correctly calculate the case of highly charged ions, and are also used to evaluate appropriate effective cross sections. As will be further explained in Sec. II B 3, computing first the relative population of $Y(n_{1s},n_{2s},n_{2p},x)$-type configurations enables us to evaluate the effective cross sections for $n = 1,2$, and 3 prior to calculating populations in the 209 final configurations. The same

TABLE I. Characteristics of various versions of ETACHA that are discussed and compared with experimental data in this paper.

ETACHA code version	Number of shells	Calculated fractions	Number of fractions	Total number of configurations
ETACHA23	3	$Y(n_{1s},n_{2s},n_{2p})$ $Y(n_{3s})$ $Y(n_{3p})$ $Y(n_{3d})$	63 3 7 11	84
ETACHA3	3	Same as above plus $Y(n_{12},n_3)$	209	$84+209=293$
ETACHA34	4	Same as above plus $Y(n_4)$	33	$293+33=326$
ETACHA4	4	Same as above plus $Y(n_{123},n_4)$	$29\times33=957$	$326+957=1283$

considerations apply to the calculation of partial populations of configurations when upper states are considered.

Similarly, then, we developed two versions of the code for ions with up to 60 orbital states of electrons, both starting with the computation of the 293 fractions of ETACHA3. The simplest is the ETACHA34 version where, in addition to the fractions of ETACHA3, the 33 fractions of the type $Y(n_4,x)$ are calculated and combined with the 209 $Y(n_{12},n_3,x)$ correlated fractions. This means that a set of $293+33=326$ rate differential equations are solved. Finally, the uppermost version, ETACHA4, considers the 957 fractions (29×33) of the type $Y(n_{123},n_4,x)$, leading to the most sophisticated version, at present, where a set of 1283 coupled rate equations have to be solved, at the expense of some computing time. However, it is worth mentioning that to fully handle ions carrying up to 60 electrons, excitation and decay processes implying upper states should be taken into account (see Sec. II B 2). Table I summarizes the characteristics of various versions of the ETACHA code. The final charge-state distribution is eventually calculated by summing over all configurations with the same number of electrons. For instance, we use for ETACHA4 the following sum:

$$P(Q,x)=\sum_{n_{123}+n_4=Z_p-Q} Y(n_{123},n_4,x). \tag{3}$$

B. Cross sections of the elementary processes

1. *Beyond the perturbative regime for projectile states from $n=1$ to 4*

Our previous version of the ETACHA code [4] was well suited to a high-velocity and low-perturbation regime, the aim being to optimize the production of high charge states after the stripping solid foil. Therefore, the first (or plane-wave) Born approximation (PWBA) can be safely used for ionization and excitation [14,15], whereas the continuum distorted-wave (CDW) approximation [16] reproduces very well the capture cross sections. However, beside the number of states that needs to be included to handle projectile ion states up to $n=4$, the extensions of the ETACHA code intend also to tackle collision systems in the nonperturbative regime in which those theoretical approaches are well known to fail in reproducing experimental results. In this respect, one can define the projectile perturbation parameter K_p:

$$K_p=\frac{Z_t}{Z_p}\frac{v_e}{v_p}, \tag{4}$$

where Z_t and Z_p are the target and projectile atomic numbers, v_e the mean orbital velocity of the active electron, and v_p the projectile velocity. Accordingly, the collision distortion will increase with K_p, but for a given collision system (i.e., Z_p impinging on Z_t at v_p), the K_p parameter decreases, with increasing principal quantum number n when considering ionization or intershell excitation of the projectile state. Hence, within the new ETACHA code versions, we improved the theoretical description of the ionization and excitation processes by introducing the continuum distorted-wave-eikonal initial state (CDW-EIS) approximation [17,18] and the symmetric eikonal (SEIK) model [19,20], respectively. Indeed, although in those two formulations, the multielectronic system (i.e., the projectile) is reduced to an effective monoelectronic one, assuming that the nonionized electrons remain frozen in their initial orbitals, those two approaches lead to a much better agreement with experiment than does the PWBA, as illustrated in Figs. 2 and 3.

On Fig. 2, the deviation of the PWBA at low velocity is clearly visible in the ionization cross section, even for $K_p<1$, and increases with the collision distortion, i.e., with the disruptive collision partner, as a result of the increase in the K_p parameter at a given projectile energy. Similar behavior is reported in Fig. 3 for the evolution of the $1s-2p$ excitation cross section for Ar^{17+} ions at $v_p=23$ a.u. colliding with neutral targets of increasing atomic number. Here the PWBA starts overestimating cross sections for K_p values above 0.4, whereas the SEIK model reproduces well the experiment up to K_p values larger than 2 [21,22].

Similar problems arise for the nonradiative capture when reaching lower velocities than previously considered. Figure 4 shows a comparison of measured cross sections (a compilation from [23–25]) for the simple and well-documented system of proton on hydrogen with the result of the relativistic capture eikonal calculation (CEIK) [26] and the CDW approximation [16]. Although none of those theories reproduces well the existing data over the whole range of the velocity domain, one sees that the CDW approximation diverges rapidly at low

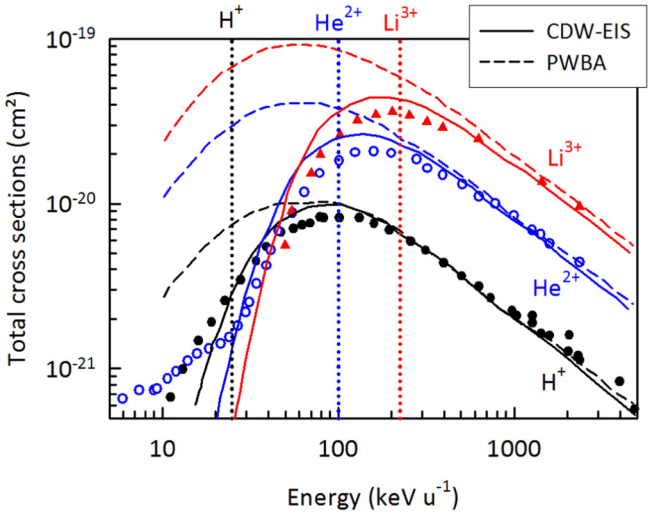

FIG. 2. (Color online) Ionization cross section of He as a function of projectile velocity induced by different disruptive collision partners, namely, H^+, He^{2+}, Li^{3+} [18]. Symbols: experimental data; dashed lines: PWBA calculations; full line: CDW-EIS calculations; the vertical dotted lines indicate when $K_p = 1$ in black for H^+, in blue for He^{2+}, and in red for Li^{3+}.

velocities whereas the CEIK calculation does quite well down to energies of a few keV and is in rather good agreement also at high projectile energy.

Of course it would be more accurate to make use of close-coupling calculations [27] in the collision regime where the perturbation parameter K_p is larger than 1. Nevertheless it would be too demanding in computing time, and as can be seen, when comparing Figs. 5 and 6, the CEIK approximation provides partial n populations in accordance with what can be expected at low velocity, while CDW calculations visibly diverge for high n values. Indeed, the CEIK model leads

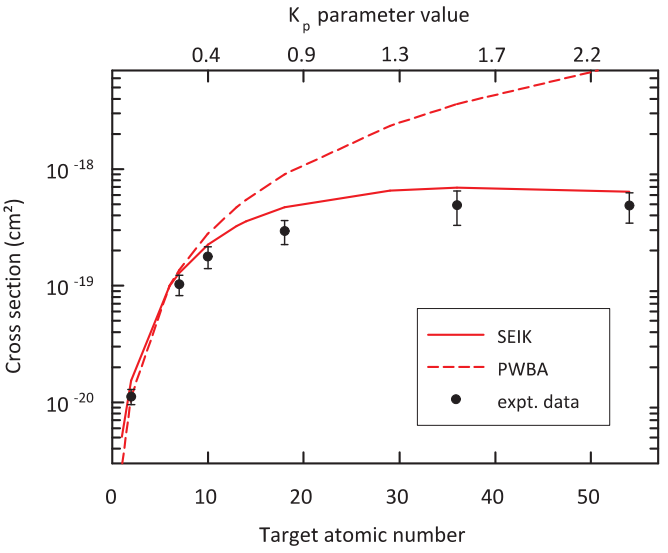

FIG. 3. (Color online) $1s-2p$ excitation cross section for Ar^{17+} ions at a fixed velocity $v_p = 23$ a.u. (13.6 MeV u^{-1}) as a function of exciting target atomic number. Dots with error bars, experiment [21]; dashed line, PWBA calculation; full line, symmetric eikonal theory.

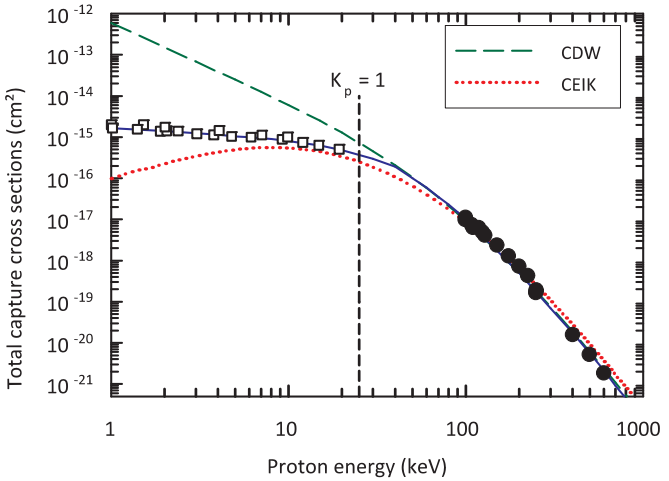

FIG. 4. (Color online) Total capture cross sections for protons in hydrogen as a function of the projectile energy: symbols for compilation of experimental data from [23] (squares) and from [24] (circles); dashed and dotted lines for theories in the CDW approximation and CEIK model, respectively.

to total cross sections that can be favorably compared to the well-known classical-over-the-barrier (COB) or reaction window within the Landau-Zener models [28,29], both shown to provide a good order of magnitude when compared to experimental data on total as well as partial n capture cross sections, even for symmetric collision systems at low velocity [30,31].

Accordingly, in every new ETACHA code version, cross sections are calculated in the following way:

(1) Ionization cross sections corresponding to $1s$, $2s$, $2p$, $3s$, $3p$, and $3d$ subshells and the $n = 4$ shell are first calculated in the plane-wave Born approximation [14,15], using screened hydrogenic wave functions for the initial states of the projectile electrons. Screening and antiscreening effects by target electrons are also taken into account in an approximate

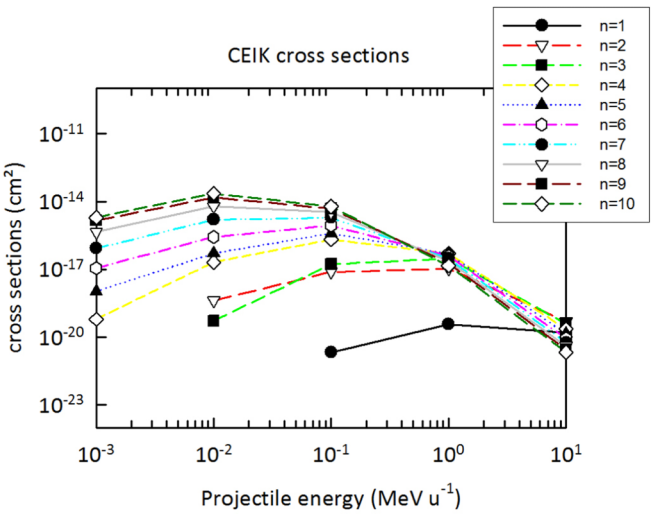

FIG. 5. (Color online) Capture cross sections for Ar^{18+} on C calculated in the CEIK approximation [26] for each n level as a function of projectile energy.

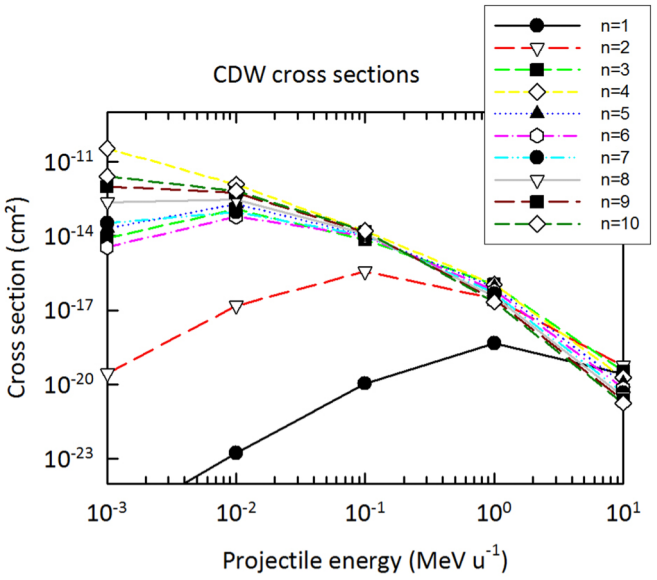

FIG. 6. (Color online) Capture cross sections for Ar^{18+} on C calculated in the CDW approximation [16] for each n level as a function of projectile energy.

way [32,33], although a better screening contribution could be calculated [34] at the expense of increased computational time. This preliminary calculation is done for computational reasons that will be explained in Sec. II B 3. As mentioned above, distortion effects at intermediate velocities ($K_p \approx 1$) have to be taken into account. This is achieved by going beyond the use of any scaling law on total cross sections as reported in [35] and by integrating the CDW-EIS equation [6,7] routine directly in the code to calculate the ionization. Unfortunately, form factors for the CDW-EIS calculation are available only for ionization in $1s$, $2s$, and $2p$ shells. We then make use of the well-known quasihydrogenic Z/n scaling approximation [36]; i.e., for $n = 3$, $\sigma(n = 3, Z) \approx \sigma(n = 1, Z/3)$, and for $n = 4$, we rather apply similar scaling $\sigma(n = 4, Z) \approx \sigma(n = 2, Z/2)$ that appears to give slightly better results.

(2) Excitation cross sections are calculated in a similar way to ionization ones, accounting for screened hydrogenic wave functions for both initial and final projectile states. Here, the saturation behavior when distortion increases is taken into account by using the SEIK approximation [19,20]. Calculated cross sections include direct and inverse intershell processes from and to all subshells in $n = 1$, 2, 3, and 4, as well as intrashell ("ℓ mixing") for $2s$-$2p$, $3s$-$3p$, and $3p$-$3d$.

(3) Nonradiative capture (NRC, or for mechanical electron capture MEC) cross sections can be accurately calculated within the continuum distorted-wave approximation at large velocities [16]. Such calculations, however, require relatively large computing time and they appear to diverge at low velocities as discussed above. We thus use the much more simple but accurate enough relativistic eikonal approximation (CEIK) as suggested by Meyerhof *et al.* [26]. We have found that, in most cases, its predictions agree well enough with CDW data at high velocity (see Figs. 4–6), and provide quite reliable values at lower velocities.

Finally, the radiative electron capture (REC) as well as radiative and Auger decay rates are treated as in the previous version of ETACHA [4]. Explicitly, the REC cross sections are calculated using the Bethe-Salpeter formula [37] and added to NRC cross sections. They are generally negligible for $n \geqslant 3$. On the other hand, partial or total radiative and Auger decay rates in one-electron ions or singly ionized atoms are taken from the literature [35,38]. A scaling procedure proposed by Larkins [39] has previously been used successfully to account for a variation of excited-state decay rates with the number of available electrons or vacancies in K, L, and M shells [13,40]. This procedure is used in ETACHA to calculate radiative and Auger decay rates, taking into account the effective (screened) nuclear charge given by the simple Slater empirical rules [41].

2. *Contribution of projectile states above* $n = 4$

In our previous version of ETACHA, excitation cross sections to $n \geqslant 4$ were estimated from $\sigma_{\rm exc}(n = 4)$, using a $1/n^3$ scaling law, and their sum added to the ionization cross sections of initial states. Such "net ionization" cross sections, however, overestimate what must be used as "effective" cross sections. Although, in such cases, the exact value of the factor to be used for estimating effective cross sections is not easy to predict *ab initio*, its value can be qualitatively understood. Indeed, adding excitation cross sections to ionization ones means that electrons in excited states are supposed to be lost immediately (that is much faster than they may deexcite). Figure 7 shows the evolution of PWBA ionization cross sections with the n principal quantum number for 28.9 MeV u^{-1} Pb^{81+} on carbon targets, as an example. Whereas the cross section increases very fast between $n = 1$ and $n = 2$, this is much less true when comparing $n = 3$ and $n = 4$. Therefore, the ionization cross section in $n = 4$ cannot at all be considered as infinite in comparison with $n = 3$, and this process cannot be assumed to take place on a negligible time scale. In contrast, the larger the principal quantum number, the more similar are ionization cross sections in neighboring shells. According to these generic trends, in the new versions of ETACHA23 or 3,

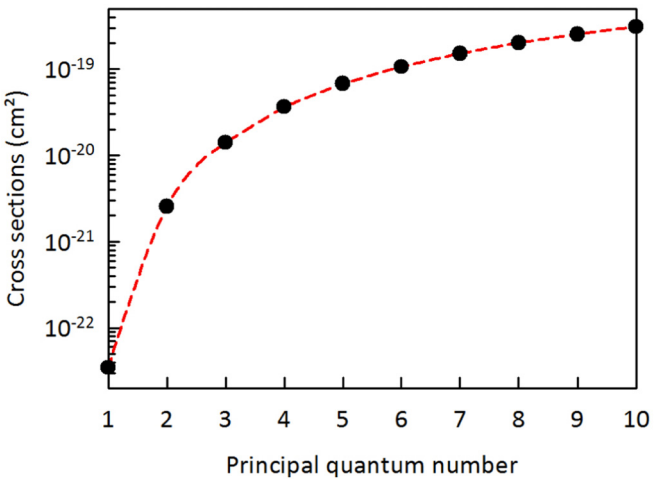

FIG. 7. (Color online) Evolution of PWBA ionization cross sections with the principal quantum number n for 28.9 MeV u^{-1} Pb^{81+} on carbon targets.

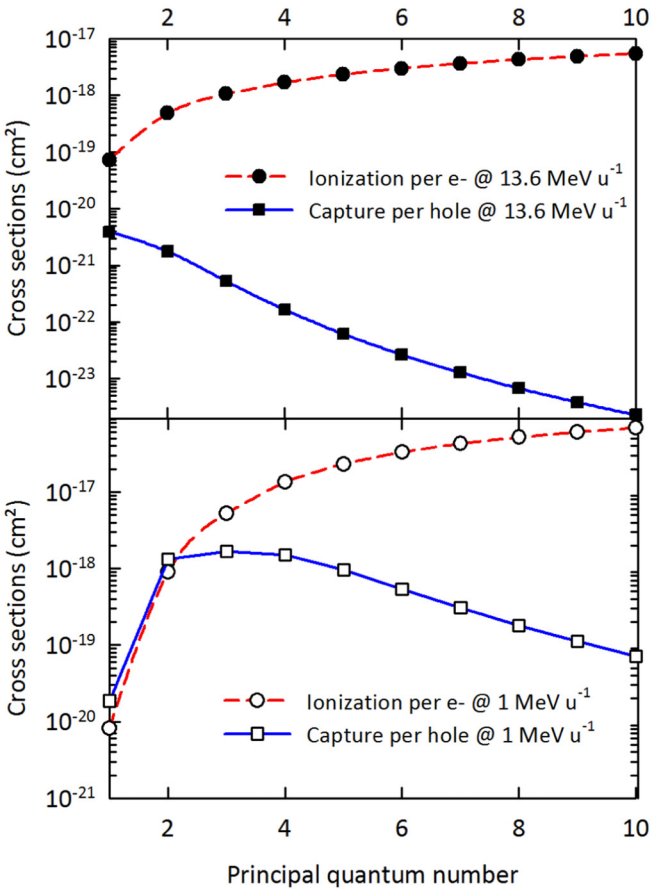

FIG. 8. (Color online) Evolution, with the principal quantum number n, of capture (per hole) and loss (per electron) cross sections, calculated within CEIK model (full line) for Ar^{18+} and PWBA (dashed line) for Ar^{17+} on C at 13.6 and 1 MeV u^{-1}.

only excitation cross sections to $n = 4$ have been added to ionization (but not the summed excitation cross sections in $n \geqslant 4$, using a $1/n^3$ scaling law as was done before). Likewise, excitation cross sections in $n \geqslant 5$ are not added to ionization at all, in the new versions of ETACHA34 and 4.

Regarding the electron capture process in the current versions of ETACHA34 or 4, only capture cross sections up to $n = 4$ are considered. However, electron populations in $n \geqslant 5$ shells may have to be considered when decreasing the projectile velocity and it could be that capture in these states should also be taken into account. Nevertheless, similarly to excitation processes in $n \geqslant 5$ shells, capture in excited states cannot be simply added to capture in $n = 4$. Figure 8 shows the evolution, with the principal quantum number n, of capture (per hole) cross sections calculated within the CEIK model for Ar^{18+} projectile and loss (per electron) cross sections within the PWBA for Ar^{17+}, impinging on carbon targets at two energies, i.e., 13.6 MeV u^{-1}, a case thoroughly considered in our previous paper [4], and 1 MeV u^{-1}, a much lower-velocity case.

These curves give the general trend to be expected when velocity is decreasing: capture increases faster than ionization, and populates more and more excited states. Nevertheless, capture "saturates" at some given n principal quantum numbers (or peaks at a given window of highly excited n states), whereas ionization continuously increases. The mean number of electrons in a given shell, being given in first approximation by the ratio between capture and ionization (times the degeneracy of the state), decreases rapidly with n, and just adding capture in excited levels to capture in $n = 3$ for ETACHA23 or 3, and in $n = 4$ for ETACHA34 or 4, would lead to an overestimate of this number of electrons. Therefore, as for excitation cross sections, electron capture in excited levels other than those included in the corresponding ETACHA version is not taken into account. One should note that this effect is not yet properly considered since it would probably necessitate inclusion explicitly of the $n = 5$ shell in the next ETACHA version.

3. *Consideration of projectile charge change, and energy loss, through the solid target*

Calculated ionization cross sections refer only to hydrogenlike ions. For lower charge states (i.e., a many-electron projectile), we make use of the independent-electron approximation which assumes the ionization cross sections to be proportional to the number of electrons in a specific shell or subshell. Effective nuclear charges are also applied to account for large changes in the cross sections for many-electron ions, and of course the effect is stronger for $n = 4$ than for $n = 1$ as shown in Fig. 9. For instance, ionization cross section *per electron* in $n = 4$ for 28.9 MeV u^{-1} Pb^{81+} is more than ten times smaller than in neutral Pb (see the bottom part of Fig. 9) and the factor is about 4 between Pb^{53+} and Pb^{22+}, which correspond to an ion with one electron in the $n = 4$ or a full $n = 4$ shell, respectively. It leads to a total factor of 128 (4×32) when all the 32 electrons in $n = 4$ shell are considered. This implies that a single set of cross sections cannot be used throughout the target thickness, but on the contrary has to be periodically recalculated, not only to account for the energy loss, but also for the charge change, as will be explained in the following.

Figure 9 shows the evolution with charge state of the projectile ionization cross section *per electron* in $n = 1$ and $n = 4$ shells for 28.9 MeV u^{-1} Pb^{q+} in carbon, taking into account screening effects in the PWBA or in the CDW-EIS approach. As expected, the reduction in cross section between the two methods, due to "strong" collision distortion (i.e. the K_p parameter, Eq. (4)), is larger, and quite significant, for $n = 1$ than for $n = 4$. On the other hand, the ratio between CDW-EIS and PWBA appears to remain almost constant over the whole range of charge state. This suggests the recipe we use in ETACHA: cross sections are first calculated both in PWBA and CDW-EIS approximation for hydrogenlike ions leading to the determination of a reduction factor, which is then applied each time a recalculation of cross sections is needed. Only PWBA type cross sections are (re)calculated, and then scaled using the reduction factor. This procedure strongly reduces the computing time.

For excitation processes, cross sections are proportional both to the number of electrons in the initial state and to the number of available vacancies in the final state. Once again, effective nuclear charges must be used, thus producing also large changes in the cross sections between the case of dressed incident ions and the one of hydrogenlike ions. Here also, SEIK cross sections are first compared with PWBA calculations

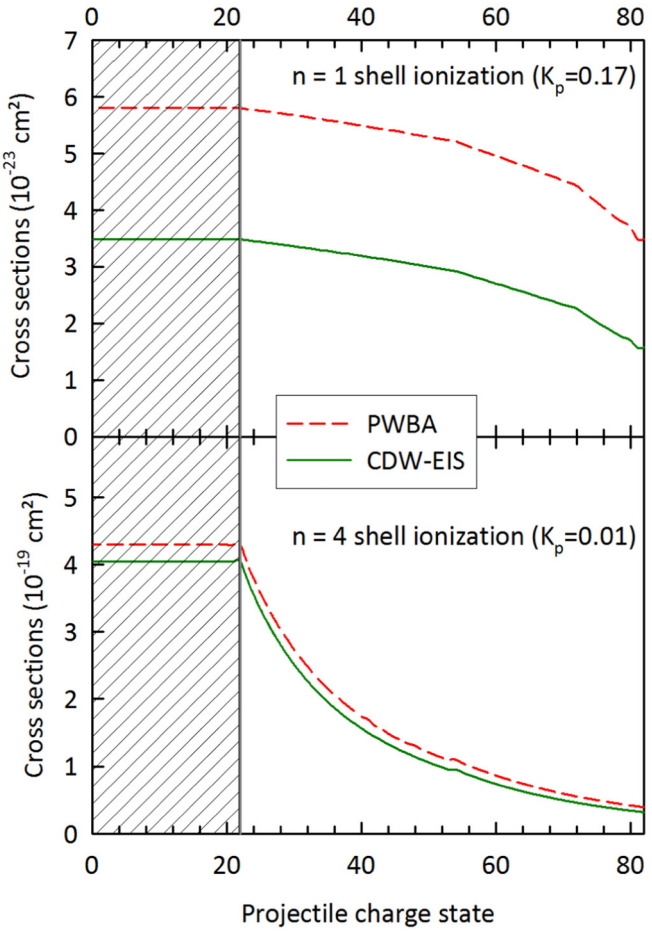

FIG. 9. (Color online) Evolution, with charge state, of the projectile ionization cross section *per electron* in $n = 1$ and $n = 4$ shells for 28.9 MeV u^{-1} Pb^{q+} in carbon as calculated with the PWBA and the CDW-EIS approach. Note that charge states below 22 (i.e., projectile with more than 60 electrons) are not taken into account.

for hydrogenlike ions in order to deduce the appropriate reduction factor that is then applied at each cross sections recalculation.

Similarly, NRC and REC cross section calculations both apply to fully stripped ions where final hydrogenic wave functions can be used. For non-fully stripped ions, we make also use of the independent electron approximation whereby capture cross sections in a specific sub-state are proportional to the number of available vacancies [13]. Moreover, effective (screened) nuclear charges are considered [39] to evaluate the energy levels of multielectron ions, further reducing capture cross sections.

C. Computing details

The program (Microsoft DIGITAL Visual FORTRAN has been used) starts with input of projectile and target characteristics (projectile atomic number, charge, mass, energy, and target atomic number, mass, density, maximum thickness). Optional calculation of coefficients accounting for projectile energy loss in target is also now provided in the new ETACHA versions [42].

Then "reference" cross sections, for capture in fully stripped ions and ionization or excitation of hydrogenlike projectile are computed. The "reduction factors" (see Sec. II B 3) for ionization and excitation processes are then calculated. At this point, results of those calculations are displayed, and it is possible to modify their values if desired.

The following step is a recalculation of all cross sections for the nonhydrogenic incident charge state. Then, as reported in Table I, the 63 differential equations for the $Y(n_{1s},n_{2s},n_{2p})$ populations and the 21 equations for $Y(n_{3s})$, $Y(n_{3p})$, and $Y(n_{3d})$ fractions are numerically integrated [43] when running the ETACHA23 version. For ETACHA3, the 209 equations for the $Y(n_{12},n_3)$ fractions are calculated; the 33 equations for $Y(n_4)$ states are considered for the ETACHA34 version. Finally the 957 equations for the $Y(n_{123},n_4)$ fractions are also numerically integrated when running the ETACHA4 version. In each case, appropriate cross sections summed and averaged over the mean populations are used; for instance, when calculating $Y(n_4)$ for uncorrelated state populations, loss rates include ionization, but also radiative and collision deexcitation processes where the mean electron numbers in $n = 1,2$, and 3 shells are taken into account. The integration step size increases with target thickness in order to provide smooth curves on a logarithmic scale. After each integration step, mean populations in each shell are recalculated, and used to recalculate the averaged cross sections. Also, all cross sections are recalculated with the appropriate new screening constants each time the mean charge state of the projectile, and/or its energy (if desired), changes by more than a few percent. Likewise, appropriate radiative and Auger decay rates are reevaluated. Finally, at each output thickness, autoionization outside the foil for each configuration is computed, and the configurations combined according to Eq. (3) (or similar formulas in other versions than ETACHA4) to produce output. The resulting files provide the charge-state distribution as a function of target thickness as well as the evolution of some selected mean substate populations.

III. RESULTS AND DISCUSSION

In what follows, we present comparisons of the different new versions of the ETACHA code, including the previous version of ETACHA23 [4] labeled as ETACHA "old," together with experimental data for different collision systems. The discussion will demonstrate the contribution of the different effects, i.e., the inclusion of more sophisticated ionization and excitation cross sections and the enlargement of the basis set, as well as the consideration of correlated configurations.

A. Comparison of the different versions of the ETACHA code for test collision systems

1. Ar^{10+} *on C at* 13.6 MeV u^{-1} ($v_p = 23$ a.u; *eight electrons on the projectile*)

Figure 10 shows the evolution of selected charge states, for Ar^{10+} on C at 13.6 MeV u^{-1} for comparison between the latest version ETACHA4, ETACHA "old," and the experimental data recorded at GANIL (the Grand Accélérateur National d'Ions Lourds in Caen, France). Here, of course, the goal was to maximize the projectile ions with the highest charge states. Although at this velocity, corresponding to

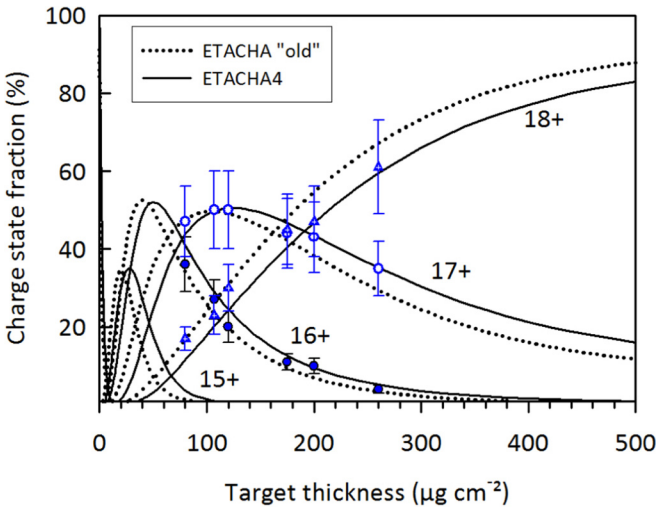

FIG. 10. (Color online) Evolution with carbon target thickness of selected charge states for 13.6 MeV u^{-1} Ar^{10+}. Symbols, experiment; dotted lines, ETACHA "old"; full lines: ETACHA4.

$K_p(\mathrm{Ar}\ 2p) \approx 0.065$ and $K_p(\mathrm{Ar}\ 1s) = 0.26$ [applying Eq. (4)], there are slight differences in the behavior of the various charge states, both code versions give rather similar results, and agree quite well with the measurements within the error bars.

2. Pb^{56+} *on C at* 28.9 MeV u^{-1} (v_p = 34 a.u.; *26 electrons on the projectile)*

In this case, one can explore not only the production of high charge states, but also the depletion of the ion incident charge that can be observed with tractable target thicknesses, unlike the previous example. On Fig. 11, the difference between the new ETACHA4 version and ETACHA "old" is visibly significant both for the diminution of the incident ion charge state and for the production of stripped ions. ETACHA4, which includes a larger basis set and more refined cross sections, leads to

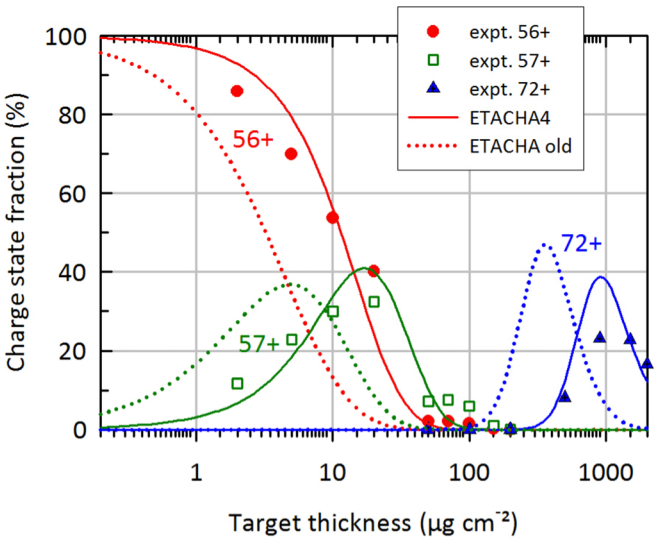

FIG. 11. (Color online) Evolution of selected charge states for 28.9 MeV u^{-1} Pb^{56+} with carbon target thickness. Symbols, experiment [42]; dotted lines, ETACHA "old"; full lines, ETACHA4.

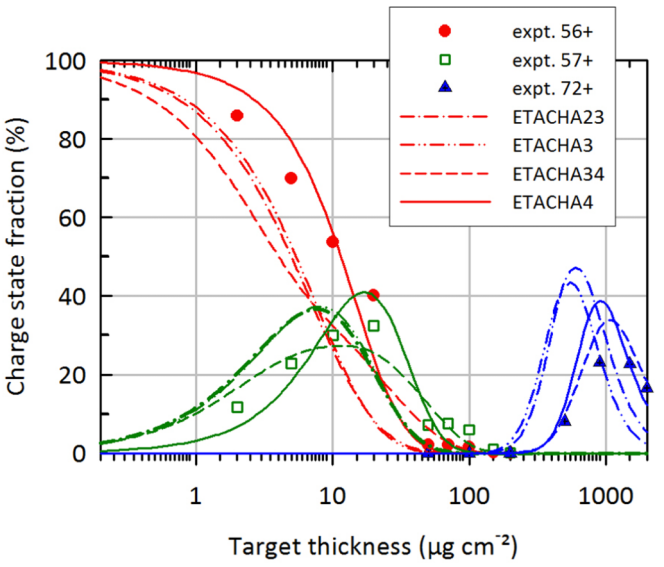

FIG. 12. (Color online) Evolution of selected charge states for 28.9 MeV u^{-1} Pb^{56+} with carbon target thickness. Symbols, experiment [42]. Dash-dotted lines, ETACHA23 model; dash-double-dotted lines, ETACHA3; short-dashed lines, ETACHA34; full lines, ETACHA4.

a clear improvement in the predictions when compared to experimental results taken from Ref. [44].

To better understand the different effects that result in this improvement, data of the four new versions of the ETACHA code are presented in Fig. 12. For this collision system, which involves a projectile initially dressed with 26 electrons (with eight electrons on the 3*d* level), the new ETACHA23 and ETACHA3 versions give very similar results. Only a slight difference is observed in the prediction of the charge state 72+ that is produced at large target thickness but neither reproduces the experimental data. Using ETACHA34 clearly improves the agreement with experimental measurements when the projectile ion starts to be stripped, i.e., for 57+ and 72+ ion charge states. Finally, as mentioned above, the ETACHA4 version gives rise to quite good predictions over the whole charge-state evolution, even at small target thickness, i.e., regarding the depletion of the 56+ charge state.

Looking in more detail at the variances between the different versions of the ETACHA code, the ETACHA34 improvement, compared to ETACHA23 and ETACHA3, in predicting stripped projectile ions is clearly due to the inclusion of $n = 4$ which plays a role not only for the capture but especially in the excitation and ionization channels. On the other hand, ETACHA34 has a tendency to underestimate the remaining fraction of the incident 56+ projectile ion at small target thickness, because of a too crude inclusion of the $n = 4$ level that indeed favored somewhat too much the electron loss. When comparing ETACHA34 and ETACHA4, at small target thickness, one can see a strong effect that can be easily explained as being due to excited states and "correlated configurations." To provide some clues as to what happens, let us take, as an example, the situation at a target thickness of 5 μg cm^{-2}, and use rounded values. According to ETACHA4, which calculates correlated configurations, the non-negligible

(i.e., larger than 1%) probabilities are

$$P(26e\text{-}_{n=1,\ 2\ \text{and}\ 3},\ \text{and}\ 0e\text{-}_{n=4}) \approx P(25e\text{-}_{n=1,\ 2,\ \text{and}\ 3},\ \text{and}\ 1e\text{-}_{n=4}) \approx 40\%,$$
$$\text{and}\ P(25e\text{-}_{n=1,\ 2,\ \text{and}\ 3},\ \text{and}\ 0e\text{-}_{n=4}) \approx P(24e\text{-}_{n=1,\ 2,\ \text{and}\ 3},\ \text{and}\ 1e\text{-}_{n=4}) \approx 10\%, \quad (5)$$

which yield $P(56+) \approx 80\%$ and $P(57+) \approx 20\%$ (see Fig. 12).

On the other hand, ETACHA34, which does not account for correlated configurations, predicts that about half of the projectile ions have 25 electrons in $n = 1,2$, and 3 and the other half 26, and also almost equal fractions (half) of ions with 0 or 1 electron in $n = 4$, according to the numbers reported in Eq. (5). However, when these probabilities are independently combined, it leads to $P(55+) \approx 0.5\times0.5 \approx 25\%$; $P(56+) \approx 0.5\times0.5 + 0.5\times0.5 \approx 50\%$, and $P(57+) \approx 0.5\times0.5 \approx 25\%$ (see Fig. 12 where the 55+ charge state is not shown, but is reported as negligibly small in measurements [42]). This feature explains the difference in behavior of ETACHA4 compared to ETACHA34 at small target thickness. It is worth mentioning that such an effect appears only for ions with electron numbers close to full shells, and for small target thicknesses where only two or three charge states have to be considered. Finally, one should note that ETACHA3 results can be made to be very close to those of ETACHA4 by "just" dividing the ionization cross section of $n = 3$ in ETACHA3 by 2. This illustrates that estimating the excitation cross section to $n \geqslant 3$, by just adding excitation cross sections in $n = 4$ to the direct ionization cross section in $n = 3$, still overestimates the "net ionization" cross section that should be used. Indeed, in this particular case of Pb^{56+} at 28.9 MeV u^{-1} on carbon, only 40% of the excitation cross section must be added to direct ionization in $n = 3$ to reproduce quite well the experimental data and to converge with ETACHA4, demonstrating, as discussed in Sec. II B 3, the difficulties of properly estimating the net ionization cross sections.

B. Results of the new ETACHA code for other benchmark collision systems

As presented in the Introduction, the main motivation to extend the ETACHA code was to be able to treat collision systems entirely out of the perturbative regime, i.e., when the perturbation parameter K_p [given by Eq. (4)] is much larger than 1. Below, we illustrate the potential of the most recent new version of the ETACHA code with two examples.

First, let us consider the collision system Pb^{56+} at 28.9 MeV u^{-1} on silicon, a target that corresponds to an increase of the perturbation K_p parameter of about 2.2. From Fig. 13, we can observe that a clear improvement is also achieved over the whole charge-state distribution when using ETACHA4 instead of ETACHA23 and comparing to experimental data obtained under a random orientation of a silicon crystal of effective thickness 1.1 μm [45], i.e., a target thickness of 327 μg cm^{-2}. It confirms the validity of ETACHA4 for treating a collision system involving a multielectron projectile. The slight variance observed beyond 72+, and similarly in Fig. 11, is most likely due to nonuniformity of the target at such thicknesses. On the contrary, the results of the new ETACHA23 version are quite unsatisfactory, even with inclusion of better

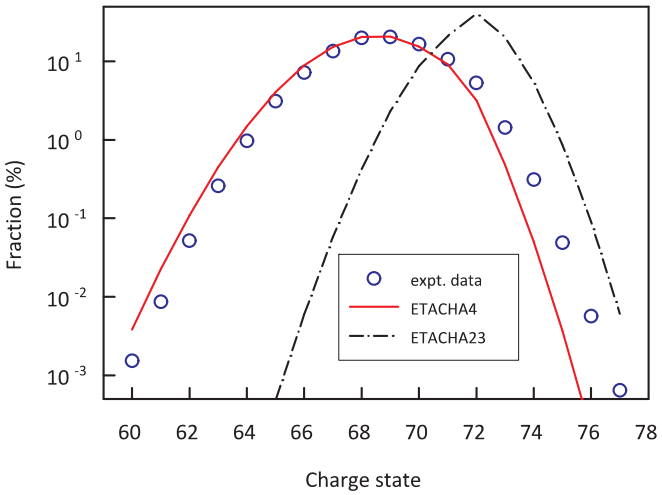

FIG. 13. (Color online) Comparison between charge-state distribution measurements of 28.9 MeV u^{-1} Pb^{56+} on a 327 μg cm^{-2} silicon target. Symbols, experiment [43]; dash-dotted lines, predictions of the new version of ETACHA23; full lines, ETACHA4.

ionization and excitation cross sections as compared to the "old" ETACHA.

It is worth noting that we have also checked the behavior of ETACHA4 in similar conditions, with measurements of still the same projectile ion, but in aluminum targets [42]. For a target thickness in a similar range (i.e., 220 μg cm^{-2} of Al), the calculated mean charge state agrees also very well with the measurements within less than 1%, reproducing also the distribution shape though it is somewhat different from that of the silicon target.

Second, we illustrate the behavior of ETACHA at low velocities, by taking the example of the mean charge-state measurements of laser-generated carbon ion beams at the exit of a 27 μg cm^{-2} aluminum target (i.e., of 100 nm) in the range of 0.045 to 0.5 MeV u^{-1} [9,46]. At 0.045 MeV u^{-1}, the K_p perturbation parameter takes a value as large as 10 for the carbon K shell, being 2.9 at 0.5 MeV u^{-1}. For those carbon beams generated by high-intensity short laser pulses passing through aluminum, the experimental data correspond to measurements of the evolution of the mean charge state (Z_{mean}) without counting the production of neutral ions, as a function of the projectile energy. To perform comparison with the ETACHA code, since we are dealing with carbon projectiles (with up to five electrons) we compute data using ETACHA3, which allows us to save computing time. As can been seen in Fig. 14, the agreement with experiment is particularly good. This example illustrates clearly the improvement of the new version due to the incorporation of the CDW-EIS and SEIK cross sections to describe ionization and excitation, respectively, in a nonperturbative regime. One can note also that ETACHA3 provides much more reliable predictions than the Shima empirical law [1], which both agree at high projectile energies (i.e., above 1 MeV u^{-1} in this case).

IV. CONCLUSIONS

The range of validity of the ETACHA code has been extended to lower velocities in all the different versions of the ETACHA

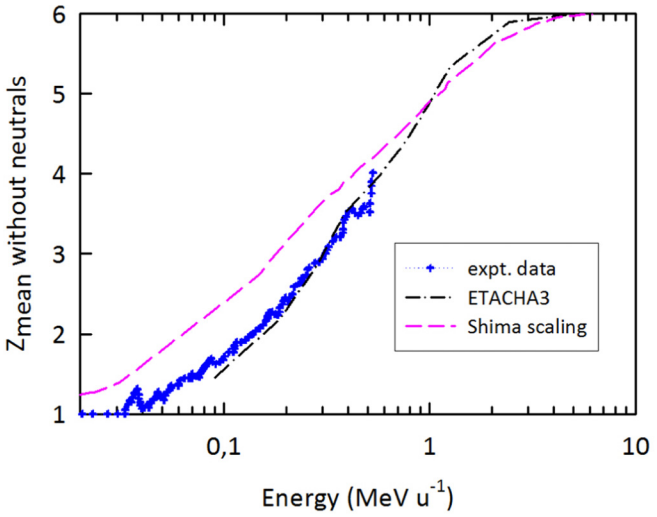

FIG. 14. (Color online) Mean charge-state measurement of laser-generated carbon ion beams at the exit of a 27 μg cm^{-2} aluminum target (symbols), compared to the ETACHA3 predictions (dash-dotted line), and to the results of Shima *et al.* [1] (dashed line).

code for projectiles with a few electrons up to dressed ions with (in principle) 60 electrons. We illustrated the different improvements that have been made, as well as the validity domain of the different available versions of the code, by comparing the corresponding computed data with test collision systems. In particular, we show that for a projectile initially dressed with 26 electrons, i.e., Pb^{56+} with eight electrons in the $3d$ level, it is mandatory to properly take into account $n = 4$ and to then make use of the ETACHA4 version. Indeed, at the projectile velocity of 23 a.u. and for relatively light targets compared to the projectile atomic number, the capture cross section in $n = 4$ is quite small, but the excitation from $n = 3$ to $n = 4$ is as large as the ionization of $n = 3$. In this respect, we can now predict with good accuracy the charge-state distribution of $^{238}U^{71+}$ at 51 MeV u^{-1} obtained after the third carbon stripper at the Riken RI-Beam factory [47]. If the target atomic number is increased or the velocity decreased, i.e., for larger K_p perturbation parameter, ETACHA4 should still be valid since the capture process is also now properly taken into account. Therefore, the ETACHA code should provide rather reliable data for some of the collision systems envisaged to cover the entire ^{100}Sn region with the Super Spectrometer Separator at SPIRAL2, as for $^{58}Ni^{19+}$ on ^{40}Ca, ^{46}Ti, ^{50}Cr, or ^{54}Fe from 3.5 to 4.5 MeV u^{-1} [8]. Nevertheless, preliminary comparisons between ETACHA and measurements performed with 11 MeV u^{-1} U^{38+} ions impinging on carbon targets (a system of importance for the design of the Rare Isotope Accelerator driver linac at Michigan State University (MSU)) [48] exhibit the requirement to even extend the ETACHA code towards the inclusion of $n \geqslant 5$. Although ETACHA4 can in principle be applied to ions with up to 60 electrons (a full $n = 4$ shell), to correctly account for the $n + 1$ level is mandatory. Future work, based on the investigations we performed, will include new tricks allowing us to fulfill this task simply enough.

On the other hand, we have shown that ETACHA3 is now well suited (running within a few seconds) to predict the mean charge state of laser-generated carbon ion beams at the exit of aluminum targets down to quite low projectile velocity (i.e., $v_p = 1.3$ a.u.). Here, the inclusion of more appropriate theories to describe ionization and excitation processes, namely, including CDW-EIS and SEIK, enables us to cover the nonperturbative energy regime.

Finally, studies are currently under way to be able to treat, within the ETACHA code, gaseous strippers as well. It corresponds also to a strong demand for the "next-generation" facilities such as RIKEN RI-beam factory (RIBF), FAIR at GSI, and FRIB at MSU in order to provide high-intensity uranium beams with energies higher than 200 MeV u^{-1} [49].

ACKNOWLEDGMENTS

The authors would like to thank J. Reading from Texas A&M, College Station and J. Nolen and J. Song from Argonne National Laboratory for their very fruitful discussions. We would like also to acknowledge the work done by Kamal Sharkas during his internship in our group. This work has been supported by the ECOS-Sud collaborative program under Contract No. A98E02 and by the French National Agency of Research under Contract No. ANR-13-IS04-0007.

[1] K. Shima, T. Ishihara, and T. Mikumo, Nucl. Instrum. Methods Phys. Res. **200**, 605 (1982).
[2] G. Schiwietz, K. Czerski, M. Roth, F. Staufenbiel, and P. L. Grande, Nucl. Instrum. Methods Phys. Res., Sect. B **225**, 4 (2004).
[3] C. Scheidenberger, T. Stöhlker, W. E. Meyerhof, H. Geissel, P. H. Mokler, and B. Blank, Nucl. Instrum. Methods Phys. Res., Sect. B **142**, 441 (1998).
[4] J. P. Rozet, C. Stephan, and D. Vernhet, Nucl. Instrum. Methods Phys. Res., Sect. B **107**, 67 (1996).
[5] M. Toulemonde, W. Assmann, C. Trautmann, and F. Grüner, Phys. Rev. Lett. **88**, 057602 (2002).
[6] E. Fokas, G. Kraft, H. An, and R. Engenhart-Cabillic, Biochimica et Biophysica Acta **1796**, 216 (2009).
[7] T. Liamsuwan and H. Nikjoo, Phys. Med. Biol. **58**, 673 (2013).
[8] http://pro.ganil-spiral2.eu/spiral2/what-is-spiral2
[9] M. Gauthier, Ph.D. thesis, Ecole Polytechnique, https://tel.archives-ouvertes.fr/pastel-00877875/document
[10] C. Vockenhuber, J. Jensen, J. Julin, H. Kettunen, M. Laitinen, M. Rossi, T. Sajavaara, O. Osmani, A. Schinner, P. Sigmund, and J. Whitlow, Eur. Phys. J. D **67**, 145 (2013).
[11] R. K. Karn, C. N. Mishra, N. Ahmad, S. K. Saini, C. P. Safvan, and T. Nandi, Rev. Sci. Instum. **85**, 066110 (2014).
[12] A. Frank, A. Blažević, V. Bagnoud, M. M. Balsko, M. Börner, W. Cayzac, D. Kraus, T. Heßling, D. H. H. Hoffmann, A. Ortner, A. Otten, A. Pelka, D. Pepler, D. Schumacher, An. Tauschwitz, and M. Roth, Phys. Rev. Lett. **110**, 115001 (2013).

[13] J. P. Rozet, A. Chetioui, P. Piquemal, D. Vernhet, K. Wohrer, C. Stephan, and L. Tassan-Got, J. Phys. B **22**, 33 (1989).
[14] G. S. Khandelwal, B. H. Choi, and E. Merzbacher, At. Data Nucl. Data Tables **1**, 103 (1969).
[15] B.-H. Choi, Phys. Rev. A **7**, 2056 (1973).
[16] D. Belkić, R. Gayet, and A. Salin, Comput. Phys. Commun. **32**, 385 (1984).
[17] P. D. Fainstein, V. H. Ponce, and R. D. Rivarola, Phys. Rev. A **36**, 3639 (1987).
[18] P. D. Fainstein, V. H. Ponce, and R. D. Rivarola, J. Phys. B **24**, 3091 (1991).
[19] G. H. Olivera, C. A. Ramírez, and R. D. Rivarola, Phys. Rev. A **47**, 1000 (1993).
[20] C. A. Ramírez and R. D. Rivarola, Phys. Rev. A **52**, 4972 (1995).
[21] D. Vernhet, J. P. Rozet, K. Wohrer, L. Adoui, C. Stéphan, A. Cassimi, and J. M. Ramillon, Nucl. Instrum. Methods Phys. Res., Sect. B **107**, 71 (1996).
[22] D. Vernhet, L. Adoui, J. P. Rozet, K. Wohrer, A. Chetioui, A. Cassimi, J. P. Grandin, J. M. Ramillon, M. Cornille, and C. Stephan, Phys. Rev. Lett. **79**, 3625 (1997).
[23] M. W. Gealy and B. Van Zyl, Phys. Rev. A **36**, 3091 (1987).
[24] P. Hvelplund and A. Andersen, Phys. Scr. **26**, 375 (1982).
[25] W. Schwab, G. B. Baptista, E. Justiniano, R. Schuch, H. Vogt, and E. W. Weber, J. Phys. B **20**, 2825 (1987).
[26] W. E. Meyerhof, R. Anholt, J. Eichler, H. Gould, C. Munger, J. Alonso, P. Thieberger, and H. E. Wegner, Phys. Rev. A **32**, 3291 (1985).
[27] W. Fritsch and C. D. Lin, Phys. Rep. **202**, 1 (1991).
[28] H. Ryufuku, K. Sasaki, and T. Watanabe, Phys. Rev. A **21**, 745 (1980).
[29] K. Taulbjerg, J. Phys. B **19**, L367 (1986).
[30] H. Tawara, E. Takacs, T. Suta, K. Makonyi, L. P. Ratliff, and J. D. Gillaspy, Phys. Rev. A **73**, 012704 (2006).
[31] M. Trassinelli, C. Prigent, E. Lamour, F. Mezdari, J. Mérot, R. Reuschl, J. P. Rozet, S. Steydli, and D. Vernhet, J. Phys. B **45**, 085202 (2012).
[32] J. H. McGuire, N. Stolterfoht, and P. R. Simony, Phys. Rev. A **24**, 97 (1981).
[33] R. Anholt, Phys. Rev. A **31**, 3579 (1985).
[34] P. L. Grande, G. Schiwietz, G. M. Sigaud, and E. C. Montenegro, Phys. Rev. A **54**, 2983 (1996).
[35] R. D. DuBois, E. C. Montenegro, and G. M. Sigaud, in *Application of Accelerators in Research and Industry: Twenty-Second International Conference*, edited by F. D. McDaniel, B. L. Doyle, G. A. Glass, and Y. Wang, AIP Conf. Proc. No. 1525 (AIP, New York, 2013), p. 679.
[36] D. Röschenthaler, H. D. Betz, J. Rothermel, and D. H. Jakubassa-Amundsen, J. Phys. B **16**, L233 (1983).
[37] H. B. Bethe and E. E. Salpeter, *Quantum Mechanics of One- and Two-Electron Atoms*, 1st ed. (Academic Press, New York, 1957).
[38] M. O. Krause, J. Phys. Chem. Ref. Data **8**, 307 (1979).
[39] F. P. Larkins, J. Phys. B **4**, L29 (1971).
[40] J. P. Rozet and A. Chetioui, J. Phys. B **14**, 73 (1981).
[41] J. C. Slater, Phys. Rev. **36**, 57 (1930)
[42] We use a FORTRAN version of Ziegler's BASIC program STOP, which compared to the present SRIM (http://www.srim.org/) provides reliable enough estimations for the evolution of the charge state distribution.
[43] D. Kahaner, C. Moler, and S. Nash, *Numerical Methods and Software* (Prentice-Hall, Englewood Cliffs, NJ, 1989).
[44] A. Leon, S. Melki, D. Lisfi, J. P. Grandin, P. Jardin, M. G. Suraud, and A. Cassimi, At. Data Nucl. Data Tables **69**, 217 (1998).
[45] A. L'Hoir, L. Adoui, F. Barrue, A. Billebaud, F. Bosch, A. Bräuning-Demian, H. Bräuning, A. Cassimi, M. Chevallier, C. Cohen, D. Dauvergne, C. E. Demonchy, L. Giot, R. Kirsch, A. Gumberidze, C. Kozhuharov, D. Liesen, W. Mittig, P. H. Mokler, S. Pita, J.-C. Poizat, C. Ray, P. Roussel-Chomaz, H. Rothard, J.-P. Rozet, Th. Stöhlker, M. Tarisien, E. Testa, S. Toleikis, M. Toulemonde, and D Vernhet, Nucl. Instrum. Methods Phys. Res. B **245**, 1 (2006).
[46] M. Gauthier, S. N. Chen, A. Lévy, P. Audebert, C. Blancard, T. Ceccotti, M. Cerchez, D. Doria, V. Floquet, E. Lamour, C. Peth, L. Romagnani, J.-P. Rozet, M. Scheinder, R. Shepherd, T. Toncian, D. Vernhet, O. Willi, M. Borghesi, G. Faussurier, and J. Fuchs, Phys. Rev. Lett. **110**, 135003 (2013).
[47] H. Ryuto, H. Hasebe, S. Yokouchi, N. Fukunishi, A. Goto, M. Kase, and Y. Yano, in *Proceedings of the 18th International Conference on Cyclotrons and Their Applications* (INFN-LNS, Giardini Naxos, Italy, 2007), p. 314.
[48] E. Kanter, J. Nolen, D. H. Youngblood, Y.-W. Lui, H. L. Clark, Y. Tokimoto, X. Chen, and R. L. Watson, Argonne National Laboratory (private communication).
[49] H. Kuboki, H. Okuno, S. Yokouchi, H. Hasebe, T. Kishida, N. Fukunishi, O. Kamigaito, A. Goto, M. Kase, and Y. Yano, Phys. Rev. Spec. Top.-Accel. Beams **13**, 093501 (2010).